

# Ripening during magnetite nanoparticle synthesis: Resulting interfacial defects and magnetic properties

Alex J. Barker

*Department of Mechanical Engineering, University of Colorado, UCB 427, Boulder, Colorado 80309*

Brant Cage and Stephen Russek

*National Institute of Standards and Technology (NIST), Boulder, Colorado 80305*

Conrad R. Stoldt<sup>a)</sup>

*Department of Mechanical Engineering, University of Colorado, UCB 427, Boulder, Colorado 80309*

(Received 6 May 2005; accepted 9 August 2005; published online 30 September 2005)

The structure and magnetic properties of magnetite ( $\text{Fe}_3\text{O}_4$ ) nanoparticles synthesized by a solvothermal processing route are investigated. The nanoparticles are grown from the single organometallic precursor Fe(III) acetylacetonate in trioctylamine (TOA) solvent at 260 °C, with and without the addition of heptanoic acid (HA) as a stabilizing agent. From the temporal particle size distributions, x-ray-diffraction patterns, high-resolution transmission electron microscope tilt series experiments, and superconducting quantum interference device magnetometry, we demonstrate that HA, a strong Lewis acid stabilizing agent, slows growth processes during ripening thus reducing the formation of interfacial defects, which we observe in the TOA-only synthesis. Nanoparticles grown with HA remain single crystalline for long growth times (up to 24 h), show a focused particle size distribution for intermediate growth times (3 h), and possess a higher magnetic anisotropy ( $15.8 \times 10^4 \text{ J/m}^3$ ) than particles grown without the additional stabilizing agent. The reduced magnetic anisotropy value for the magnetite nanoparticles grown in TOA only ( $1.29 \times 10^4 \text{ J/m}^3$ ) is attributed to polycrystallinity induced by the uncontrolled ripening process. This work may have significance for contrast enhancement in magnetic resonance imaging. © 2005 American Institute of Physics. [DOI: 10.1063/1.2058191]

## I. INTRODUCTION

The size, dispersity, and crystal structure of nanoparticles in colloidal systems are critical factors that influence the bulk properties of nanoparticle ensembles.<sup>1</sup> This is especially true for magnetic nanoparticles, in which even small changes in these physical parameters can significantly modify the overall properties of the ensemble.<sup>1–5</sup> For example, the transition of a magnetic particle from the single to multidomain state is dictated by the composition, size, and shape of the particle.<sup>6</sup> Furthermore, the monodispersity and crystal structure of the particle ensemble are crucial in determining the blocking temperature, saturation magnetization, and coercivity of the magnetic system.<sup>2–4,7</sup> These properties are important for contrast enhancement in magnetic resonance imaging.

One commonly employed preparation method for high-quality magnetic nanoparticles is the solvothermal synthesis route, where the nanoparticles are nucleated and grown at elevated temperatures (150–300 °C) in a high-boiling-point solvent from one or more organometallic precursors.<sup>1,2,7–9</sup> Critical to controlling the physical properties of nanoparticles grown by this route are the choice of solvent and the inclusion of a stabilizing agent.<sup>8,10</sup> While the solvent provides a medium for particle nucleation and growth from diffusing monomers, the stabilizing agent acts to mediate particle growth through chemical interaction with the particle's

surface. In general, the processes involved with nanoparticle nucleation and growth in hot solvent are not completely understood and as a consequence, the ability to synthetically prescribe key material properties remains an experimental challenge.

Particle growth after nucleation can occur by several mechanisms. Initial growth immediately after nucleation occurs by consumption of reactant from the surrounding solution. In this mechanism, growth is rate limited by diffusion (i.e., consumption of monomer in the volume matrix) and as a result, researchers have demonstrated particle size distribution focusing through the rigorous manipulation of the early stage growth process.<sup>11</sup> After the reactant is exhausted, the particle ensemble continues to equilibrate via growth processes traditionally referred to as ripening or coarsening. Two primary growth mechanisms are commonly active to varying degrees during the ripening process. In the first growth mechanism, known as Ostwald ripening, larger particles grow at the expense of those with smaller, less stable dimensions. In the second growth mechanism, known as Smoluchowski ripening, particles grow by coalescence through convection or active mixing. The ability to manipulate particle equilibration at later times is equally important for the development of reliable, repeatable, and monodisperse particle size distributions, since growth from reactant and ensemble ripening processes often overlap during intermediate growth times. Therefore, experimental control of the equilibration process is particularly important for the prevention of unwanted ripening.

<sup>a)</sup>Electronic mail: Conrad.Stoldt@Colorado.edu

Considering the recent observation of an oriented attachment mechanism in the ripening regime of ceramic nanocrystal growth,<sup>12,13</sup> the presence of this and other defect causing equilibration processes can significantly impact the material properties of the particle ensemble during ripening. For example, ripening-based degradation of magnetic properties can occur due to interfacial defects such as grain boundaries and twinned planes common in coalescence and oriented attachment-type growth.<sup>5,14,15</sup>

In this work, magnetite ( $\text{Fe}_3\text{O}_4$ ) nanoparticles are synthesized from a single organometallic precursor in a high-boiling-point solvent. In addition, we conduct parallel experiments with a high-affinity stabilizing agent added to the solvent. These experimental systems allow us to identify and control the negative effects of ripening-based growth on nanocrystal structure and material properties. Consequently, we demonstrate that the addition of an appropriate stabilizing agent not only slows the overall growth rate, but also yields a single-crystal structure through the inhibition of nanoparticle coalescence during equilibration, thereby enhancing the end magnetic properties of the ensemble. This enhancement is shown by measurements of the magnetization as a function of the temperature and magnetic field.

## II. EXPERIMENTAL SECTION

### A. Materials

Triethylamine (98%), Fe(III) acetylacetonate (further referred to as  $\text{Fe}(\text{Acac})_3$ , 97%), heptanoic acid (99%), anhydrous toluene (99.8%), and ethanol were purchased from Aldrich. All chemicals were used as purchased from the manufacturer and no further purification steps were taken.

### B. Synthesis of $\text{Fe}_3\text{O}_4$ nanocrystallites

$\text{Fe}_3\text{O}_4$  nanocrystallites were synthesized in the absence of a secondary stabilizing agent by heating 20 ml of triethylamine to reflux (260 °C) under nitrogen gas in a three-necked round bottom flask. The solution was mixed using a magnetic stir bar. Upon reaching temperature, 0.045 M  $\text{Fe}(\text{Acac})_3$  was carefully added to the solvent. The solution immediately turned dark, opaque brown. 1.5 ml aliquots were taken from the solution at 1, 3, 6, and 24 h. The experiment was halted at 72 h by quenching the solution with toluene. The resulting product was a clear brown solvent with a black precipitate. The precipitate proceeded to agglomerate in the area surrounding the magnetic stir bar after mixing was halted.

A second experiment, similar to the first, included heptanoic acid (HA) acting as an additional stabilizing agent. For this protocol, a 20% molar concentration of heptanoic acid was added to the triethylamine. Here, 18.6 ml triethylamine and 1.4 ml heptanoic acid were heated to reflux (260 °C) according to the process described previously. 0.045 M  $\text{Fe}(\text{Acac})_3$  was carefully added to the solvent and the solution immediately turned a translucent reddish-brown color. 1.5 ml aliquots were taken from the solution at 1, 3, 6, and 24 h. The experiment was quenched with toluene after 72 h. The aliquot at 1 h yielded no precipitate and only the

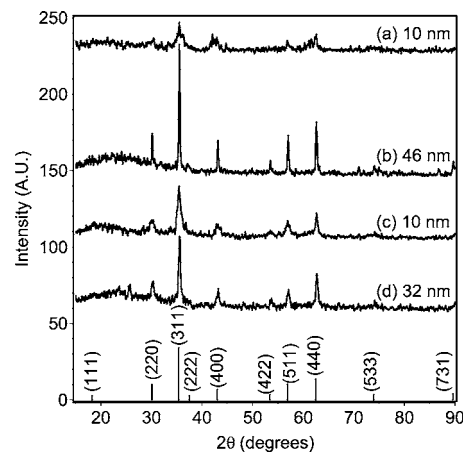


FIG. 1. XRD patterns for magnetite nanocrystallites precipitated in TOA at (a) 3 h, (b) 72 h, and in HA/TOA at (c) 3 h and (d) 72 h reaction times. Average crystallite sizes as calculated by Scherrer broadening are shown for each respective pattern. The magnetite reference spectrum is shown at the bottom of the graph for comparison.

bright red solution was visible. For aliquots that did have a precipitate, the solvent was a clear red-brown with a black precipitate. The precipitate agglomerated around the stir bar after the experiment was terminated.

All of the aliquots along with the final product from the two experiments were centrifuged at 4000 rpm for 15 min and washed three times in toluene to remove the excess organic material (Allegra X-22, SX4250 Rotor, Beckman Coulter). Precipitate obtained after centrifugation was resuspended in toluene and labeled TOA for the triethylamine-only system, and HA/TOA for the heptanoic acid/triethylamine system. In the case of samples that yielded no precipitate, the samples were kept in solution and no further steps were taken to obtain a precipitate.

### C. Characterization of materials

Powder x-ray diffraction (XRD), transmission electron microscopy (TEM), and high-resolution TEM (HRTEM) were performed on the aliquots and final product to determine the particle size, particle size distribution (PSD), and crystal structure. Powder XRD measurements were obtained using a Scintag Pad V diffractometer equipped with a Cu  $K$  radiation source ( $\lambda = 1.540562$  nm). Samples were scanned from  $2\theta = 15^\circ$  to  $2\theta = 90^\circ$  at a scan rate of 2 deg/min. TEM micrographs were obtained on a Philips CM10 operating at 80 kV. Over 1000 particles were counted from TEM micrographs taken at different areas on the carbon-coated grid to obtain each aliquot's PSD. HRTEM micrographs and tilt series experiments were performed on a FEI Tecnai TF20 electron microscope with an accelerating voltage of 200 kV. All TEM samples were prepared by placing a drop of the nanoparticle-containing solution on clean weighing paper and placing the grid on top of the drop.

For two representative samples consisting of particles synthesized after 3 h in the HA/TOA and TOA-only system, a commercial superconducting quantum interference device (SQUID) magnetometer (Quantum Design, MPMS-7) was used to perform the magnetic measurements as a function of

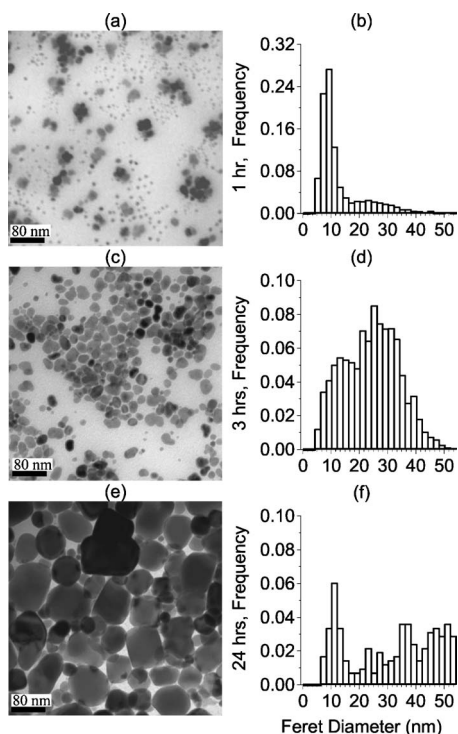


FIG. 2. Fe<sub>3</sub>O<sub>4</sub> nanoparticles synthesized in the TOA-only system: [(a) and (b)] TEM image and PSD after 1 h; [(c) and (d)] TEM image and PSD after 3 h; and [(e) and (f)] TEM image and PSD after 24 h. Note that for comparison purposes the 24 h distribution (f) was truncated at 54 nm. However, the PSD continues beyond 54 nm with a maximum particle diameter near 104 nm.

applied field and temperature. Zero-field-cooled (ZFC), field-cooled (FC), and field sweep measurements were then obtained for each sample. The ZFC and FC measurements were obtained at a field strength of  $\mu_0 H = 0.1$  T and the field sweep was obtained over the range of  $-1 \leq \mu_0 H \leq 1$  T at both 10 and 300 K.

### III. RESULTS AND DISCUSSION

In our single precursor solvothermal process, the thermal decomposition of Fe(Acac)<sub>3</sub> at 260 °C provides the source of iron and oxygen monomers for growth of the Fe<sub>3</sub>O<sub>4</sub> nucleate phase in TOA. During growth, the presence of coordinating molecules such as TOA and HA mediate monomer incorporation and stabilize growing particles, as well as prevent particle aggregation due to van der Waals and magnetic attractive forces.<sup>16</sup> The coordinating molecules preferentially adsorb on the surface of Fe<sub>3</sub>O<sub>4</sub> nucleates, effectively “capping” the inorganic phase with an organic monolayer. As a result, monomer incorporation and coarsening effects such as Ostwald ripening are either mitigated or slowed.<sup>16,17</sup> However, by way of a simple Lewis acid/base analysis, HA (the more acidic of the two coordinating molecules) will have a stronger affinity for the more basic iron oxide surface.<sup>18,19</sup> In principle, and as shown in this work, the presence of HA on the surface of the particle slows both growth by diffusion and coarsening of the particle to a significantly greater degree than a TOA-only reaction. It should be noted that in preliminary experiments not reported here, the use of biphenyl ether as a noncoordinating solvent yielded very large (approx-

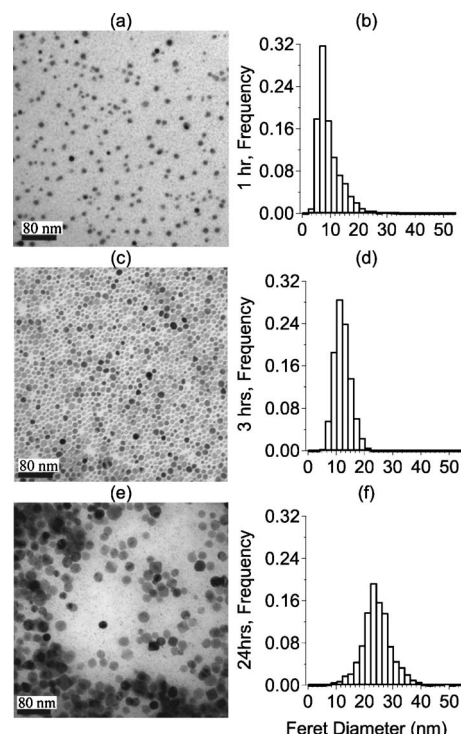


FIG. 3. Fe<sub>3</sub>O<sub>4</sub> nanoparticles synthesized in the HA/TOA system: [(a) and (b)] TEM image and PSD after 1 h; [(c) and (d)] TEM image and PSD after 3 h; and [(e) and (f)] TEM image and PSD after 24 h.

mately 200–400 nm in diameter) nanoparticle aggregates due to unrestrained coalescence during ripening.

In Fig. 1, the resulting XRD patterns from the two experiments (TOA only and HA/TOA) are shown for reaction times of 3 and 72 h. Scherrer broadening calculations at the (311), (511), and (440) peaks give the average crystallite size for the aliquots as a function of time (without considering contributions from crystal stress). TEM images are used to confirm the crystallite sizes obtained by the Scherrer analysis. In general, a close agreement between particles sizes estimated from XRD and TEM data indicates that the majority of the synthesized particles are single crystalline. However, some discrepancies between the two measurements are found in this work, the cause of which is attributed to unrestrained nanoparticle coalescence during equilibration. As seen in Fig. 1, both the TOA-only and HA/TOA reactions yield Fe<sub>3</sub>O<sub>4</sub> crystallites at 260 °C. In both cases, a reaction time of 3 h gives an average particle size of 10 nm. After a reaction time of 72 h, the average particles sizes for each experiment are seen to diverge, with the TOA-only protocol producing a larger average particle diameter with time.

TEM images and their respective PSD's are shown in Fig. 2 for nanoparticles grown by the TOA-only reaction protocol at 260 °C. When the TOA-only system is examined, the weaker coordination of TOA to the iron oxide surface yields a higher growth rate compared to the data shown for the HA/TOA system. At 1 h, the majority of the particles grown in TOA only have an average diameter near 8 nm, with a smaller population of larger particles [Figs. 2(a) and 2(b)]. After 3 h, the PSD is bimodal with a majority of the particles having an average diameter near 26 nm. As with the larger particles in Fig. 2(a), the particles grown for 3 h ap-

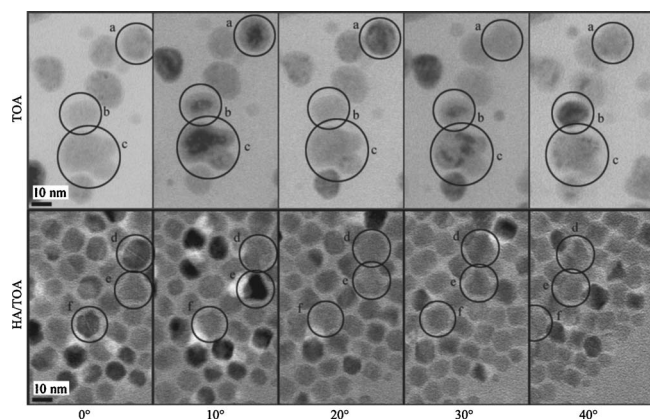


FIG. 4. HRTEM tilt series taken at 0°, 10°, 20°, 30°, and 40°. The upper row shows the TOA-only aliquot, while the lower row shows the HA/TOA aliquot series. Both aliquots were taken after a 3 h reaction period. The labeled circles follow the selected particles through the tilt series. HA/TOA particles “d” and “f” show evidence of twin defects at 0° tilt.

pear irregular in shape with very coarse edges. After 24 h, the particles grown in the TOA-only reaction become less irregular in shape than at earlier times, but show a significantly broader PSD [Figs. 2(e) and 2(f)] with diameters as large as 104 nm.

TEM images and their respective PSD's are shown in Fig. 3 for nanoparticles grown by the HA/TOA protocol at 260 °C. Particles grown for 1 h in HA/TOA appear regular in shape with relatively smooth edges, and possess a narrow PSD with an average diameter near 6 nm [Figs. 3(a) and 3(b)]. After 3 h, the particles remain regular in shape with smooth edges, and show a focused PSD with an average diameter near 10 nm [Figs. 3(c) and 3(d)]. After 24 h, the particles grown in the HA/TOA system maintain a regular, compact shape with smooth edges [Figs. 3(e) and 3(f)]. Furthermore, the PSD remains narrow when compared to the particles grown in the TOA-only reaction. From these results, it is evident that the addition of HA to the reaction acts to slow the overall nanoparticle equilibration process. This confirms our notion that growth rates are faster in the system with a lower affinity stabilizing agent.

The average crystallite size of the TOA synthesized particles as determined from the XRD spectrum [Fig. 1(a)] is only 10 nm, while the TEM and PSD data shown in Figs. 2(c) and 2(d) indicate an average particle diameter of near 22 nm. We determined that this discrepancy in the estimated size is caused by polycrystalline structure in the TOA-only particles. This conclusion is confirmed through the analysis and comparison of a HRTEM tilt series collected for the TOA-only and HA/TOA nanoparticles. The HRTEM tilt series for the TOA-only nanoparticles is shown in the upper panel of Fig. 4. The series displays irregular contrasts within the particle volume boundary during rotation, showing asymmetry within the crystal structure and confirming that the particles are indeed polycrystalline [representative particles are labeled a–c].<sup>15</sup> In contrast, the tilt series shown for the HA/TOA system in Fig. 4 displays a highly regular particle crystal structure with no asymmetric contrast within the individual particles d–f. This observation is confirmed by the magnified TEM image in Fig. 5 of a single Fe<sub>3</sub>O<sub>4</sub> nanopar-

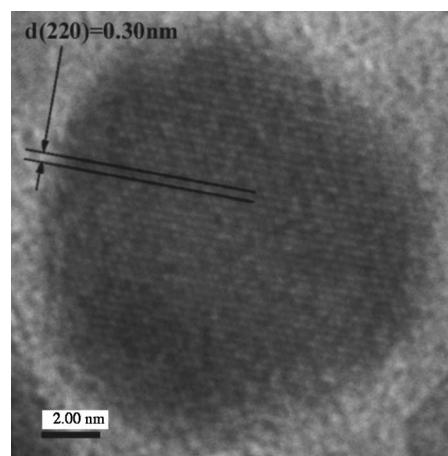


FIG. 5. Lattice fringes showing the single-crystal nature of the magnetite synthesized in HA/TOA at 3 h. The indicated lattice spacing is concurrent with magnetite's (220) plane.

ticle grown in the HA/TOA system, where the lattice fringes are resolved confirming the single-crystal nature of the particle. As shown by the tilt series and PSD evolution, the greater affinity of HA to the surface of the iron oxide appears not only to slow the growth of the particles, but also improve the nanoparticle crystal structure, preventing the formation of polycrystalline domains in the particles. The HA/TOA particles are in general single crystals; however, twinning defects are present in some of the particles as seen in particles “d” and “f” of the 0° HA/TOA tilt frame. Similar to the previous observations of highly crystalline biogenic magnetite, twin defects are seen in TEM images as a light line dissecting the particle into halves.<sup>20</sup>

The PSD of the particle sizes for the TOA-only system display a distinctly bimodal distribution at 3 h [Fig. 2(d)]. The early development of the second peak is also seen in the 1 h aliquot. It is worth noting that bimodal distributions have been observed in micelle-mediated particle syntheses under conditions where the micelle film flexibility and reagent concentration meet specific criteria.<sup>21,22</sup> Monte Carlo simulations of these micelle systems attribute the bimodality of the PSD to the operation of multiple coarsening mechanisms in the equilibration process (i.e., coalescence and Ostwald ripening).<sup>22</sup> While the parallels between micelle-based reactions and our solvothermal process are limited, it may be worth exploring in future studies the relationship between monomer concentration, capping agent affinity, and the existence of bimodal PSD's in solvothermal reactions.

The irregular shape and polycrystalline nature of the particles synthesized in TOA alone (Fig. 4, upper panel) indicates that Smoluchoski ripening is more prevalent in this system (especially at times <24 h). These polycrystals can be thought of as individual crystallites that have been incorporated into a larger particle through coalescence. Since the time scale for the coalescence is short due to mixing, there is no time for the incorporated crystals to undergo restructuring to a more energetically favorable single-crystal structure. As a consequence, the particles exhibit irregular shapes with rough edges and polycrystalline structure at short and intermediate times [Figs. 2(a) and 2(c)]. As reaction times ap-

proach 24 h, the large population of smaller particles has previously coalesced, thus forming a smaller number of large polycrystalline particles that continue to ripen with time. In this late time, low-affinity ligand scenario, Smoluchowski ripening gives way to Ostwald ripening as the dominant coarsening mechanism due to the lowered probability of particle coalescence.<sup>13</sup> This is validated by our observation at later times that restructuring via Ostwald ripening yields faceted crystalline structures with smooth edges [Fig. 2(e)], hence a more energetically favorable atomic configuration. We emphasize that unlike the polycrystalline nature early in the TOA-only synthesis, late stage XRD broadening and TEM image analyses confirms that this system at 24 h is primarily composed of large single-crystal particles.

While the TOA-only system is crystalline at 24 h as indicated by faceting in the TEM images, the PSD indicates a highly polydisperse ensemble [Figs. 2(e) and 2(f)]. This agrees with the general trend of increasing polydispersity with time as seen in the PSD's measured at 1 and 3 h. In contrast, the PSD's for the HA/TOA system shown in Fig. 3 yield the standard deviations of 54%, 28%, and 25% at 1, 3, and 24 h, respectively. This trend indicates a focusing effect similar to that observed in growth processes without coalescence.<sup>11,23</sup> As mentioned previously, the addition of HA slows nanoparticle growth and maintains a relatively narrow PSD when compared to the ever widening PSD of the TOA-only system. It should be noted that at 72 h, the HA/TOA PSD deviates from the earlier trend, and becomes highly polydisperse (not shown). This trend is previously observed by other researchers,<sup>13</sup> and possibly indicates either a boiling off or degradation of the HA stabilizing agent (BP=260 °C) after prolonged reaction times.

The Fe<sub>3</sub>O<sub>4</sub> surface is an electron pair donor or a Lewis base,<sup>19</sup> while the primary solvent (TOA) is a weak Lewis acid. As a consequence, the solvent only passively interacts with the Fe<sub>3</sub>O<sub>4</sub> surface during growth. The addition of a high-affinity stabilizing agent such as HA, a strong Lewis acid, slows the overall growth rate and prevents unwanted particle coalescence—likely due to a strong capping effect on the Fe<sub>3</sub>O<sub>4</sub> surface. The capping of the Fe<sub>3</sub>O<sub>4</sub> surface could slow equilibration through the inhibition of either the Ostwald or Smoluchowski ripening processes.<sup>16</sup> However, as demonstrated in this work, the degree to which each of these mechanisms are active determines the amount of undesired crystalline defects. Without the addition of HA, the TOA-only reaction displays an active ripening regime characterized by rapid, unrestrained coalescence at early times, and an intermediate growth stage composed of irregular, polycrystalline particles [Fig. 2(c)]. Late stage growth in the TOA-only system is dominated by Ostwald ripening and atomic restructuring processes, which act to smooth the particle edges and remove grain boundaries through diffusion processes [Fig. 2(e)]. Therefore, we observe that the Lewis acid strength of the solvent, and the addition of a high-affinity stabilizing agent, significantly impacts the crystal structure and size distribution of the resulting nanoparticle ensemble through suppression of the various ripening processes.

Critical to any nanoparticle synthesis protocol is the resulting material properties of the ensemble, such as the mag-

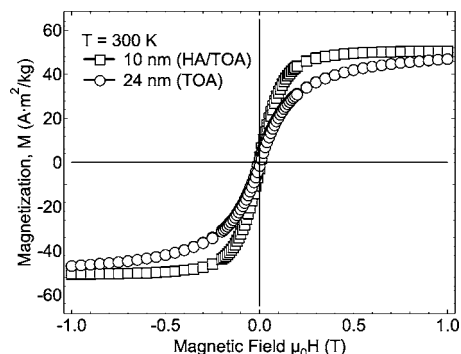


FIG. 6. Magnetization as a function of applied field measured at 300 K. The 10 nm particles ( $\square$ ) were synthesized in the presence of TOA and HA, while the 24 nm particles ( $\circ$ ) were synthesized in the presence of TOA only.

netic behavior. To this end, we have performed a comprehensive characterization of the magnetic properties of the nanoparticles synthesized in the HA/TOA and TOA-only systems. With these results, we can link the observed changes in crystal structure and size distribution to the measured magnetic properties for nanoparticles grown from differing solution chemistries.

To compare the magnetic properties resulting from the HA/TOA and TOA-only synthetic protocols, we examined the nanoparticles obtained after a synthesis time of 3 h, which yielded particles measuring 10 and 24 nm in diameter, respectively, (Figs. 3(c) and 3(d) and Figs. 2(c) and 2(d)). These samples were chosen for their relatively narrow PSD as determined over the duration of each experimental run and the differences in crystal structure observed by TEM and XRD. When considering the effects of surface spin disorders, ligand-oxide surface bonding interactions, and the finite-size effect in single crystals,<sup>7,24</sup> the 24 nm particles would normally be expected to display a larger magnetization ( $M$ ) and saturation magnetization ( $M_s$ ) than the 10 nm particles. To explore this, the  $M_s$  was obtained for each system at 300 and 10 K (Figs. 6 and 7) using a high-field fit to the expression  $M = M_s(1 - A/H^2)$ , where  $A$  is a field-independent parameter and  $H$  is the applied field. Using this relationship to calculate  $M_s$  at infinite field, the 10 nm particles measured 51 and 64 A m<sup>2</sup>/kg at 300 and 10 K, respectively (bulk magnetite = 87 A m<sup>2</sup>/kg). The 24 nm particles gave an  $M_s$  of 49 and 55 A m<sup>2</sup>/kg at 300 and 10 K, respectively. According to

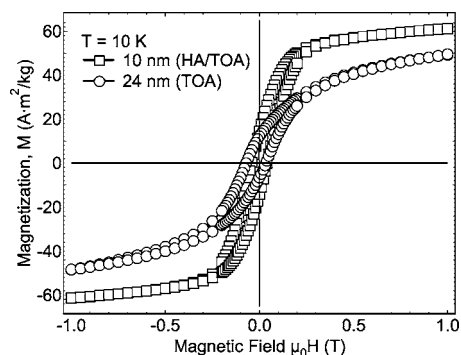


FIG. 7. Magnetization as a function of applied field measured at 10 K. The 10 nm particles ( $\square$ ) were synthesized in the presence of TOA and HA, while the 24 nm particles ( $\circ$ ) were synthesized in the presence of TOA only.

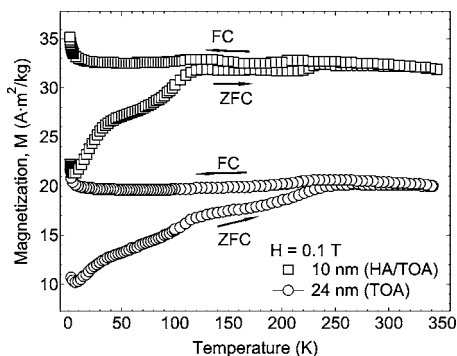


FIG. 8. Field-cooled (FC) and zero-field-cooled (ZFC) magnetization for 10 nm (HA/TOA,  $\square$ ), and 24 nm (TOA,  $\circ$ ) particles. The change in the slope on the ZFC graph indicates the Verway transition occurring over the temperature range of 100–120 K (Ref. 24).

these calculated values from the field sweep curves, the  $M_s$  for the 10 nm particles was equivalent or slightly larger than the 24 nm ensemble. Given the much larger volume of the 24 nm particles, this is significant, as discussed later and demonstrated by the large differences in the magnetocrystalline anisotropy,  $K$ . In addition, the ZFC and FC plots shown in Fig. 8 give a much higher magnetization for the 10 nm particles when compared to the 24 nm particles. This is contrary to what would be expected if both systems contained particles made up of single crystals, especially when considering the negative effects of surface spin disorders in smaller particles due to high surface-to-volume ratios. However, unlike the 10 nm single crystals obtained with the HA/TOA system, our TEM and XRD data indicate that the 24 nm particles made in the TOA-only system are actually polycrystalline with an average crystallite size of 10 nm [Fig. 1(a)]. Therefore, the polycrystalline nature of the 24 nm particles negatively affects the magnetocrystalline anisotropy  $K$  due to the increased number of grain boundaries present in each particle. Furthermore, the more polydisperse nature of the TOA-only sample may also result in the decreased  $M$  and  $M_s$  values. Therefore, we believe that the larger  $M$  and  $M_s$  values obtained are due to the single crystal, less polydisperse nature of the nanoparticles grown with a high-affinity stabilizing agent.

To validate the unexpected values of  $M$  and  $M_s$  as a function of size, the anisotropy constant  $K$  was calculated at a measurement time of 100 s, a magnetic field of 0.1 T, and an assumption of the frequency factor as  $10^9$  Hz using the relation for superparamagnetic particles,  $T_B = KV/25k$ , where  $T_B$  is the blocking temperature,  $k$  is the Boltzmann constant, and  $V$  is the particle volume.<sup>7</sup> From Fig. 8,  $T_B$  is estimated to be 240 and 270 K for the 10 and 24 nm particles, respectively. Therefore, the anisotropy constant for the 10 and 24 nm magnetic nanoparticles is  $16 \times 10^4$  and  $1.3 \times 10^4$  J/m<sup>3</sup>, respectively. The reduced anisotropy value for the larger 24 nm particles validates our counterintuitive magnetization results and is supported by the polycrystalline nature of these particles as observed by TEM.

#### IV. CONCLUSION

Magnetite nanoparticles are synthesized by solvothermal processing with and without an added stabilizing agent.

From temporal PSD and XRD analyses, HRTEM tilt series experiments, and SQUID magnetometry, we demonstrate that the negative effects of coarsening mechanisms on crystal structure can be inhibited with the appropriate inclusion of one or more stabilizing agents. By including HA, a strong Lewis acid stabilizing agent, particle growth rates in the ripening phase are slowed, thus yielding nanocrystalline particles at growth times as long as 24 h. After growth for 3 h, the PSD is observed to narrow indicating a focusing effect at intermediate times. For longer growth times, the PSD is observed to defocus, yielding a broader size distribution of single-crystalline magnetite particles. Without the inclusion of HA, growth rates are uncontrolled in the TOA-only system resulting in larger particles having a broad PSD even at short growth times (1 h) and interfacial defects such as grain boundaries. With the inclusion of a stabilizing agent such as HA, the resultant single-crystal particles grown for 3 h possess a higher magnetic anisotropy than particles grown in the TOA-only system. The reduced magnetic anisotropy value for the TOA-only system is attributed to the polycrystalline nature of the nanoparticles.

#### ACKNOWLEDGMENTS

This work was supported by the University of Colorado at Boulder and NIH Grant No. HL72738. The authors would also like to thank the Boulder Laboratory for 3D Electron Microscopy (a NIH supported National Research Resource), particularly, Richard McIntosh and Cindi Schwartz for aid in obtaining the HRTEM tilt images. We are also grateful for the help of Roy Geiss of NIST, Boulder in obtaining lattice fringe TEM images.

Note: Certain commercial instruments and materials are identified to specify the experimental study adequately. This does not imply endorsement by NIST or that the instruments or materials are the best available for the purpose.

- <sup>1</sup>C. B. Murray, C. R. Kagan, and M. G. Bawendi, *Annu. Rev. Mater. Sci.* **30**, 545 (2000).
- <sup>2</sup>S. H. Sun and C. B. Murray, *J. Appl. Phys.* **85**, 4325 (1999).
- <sup>3</sup>X. M. Lin, C. M. Sorensen, K. J. Klabunde, and G. C. Hadjipanayis, *J. Mater. Res.* **14**, 1542 (1999).
- <sup>4</sup>D. J. Zhang, K. J. Klabunde, C. M. Sorensen, and G. C. Hadjipanayis, *Phys. Rev. B* **58**, 14167 (1998).
- <sup>5</sup>D. L. Leslie-Pelecky and R. D. Rieke, *Chem. Mater.* **8**, 1770 (1996).
- <sup>6</sup>K. Fabian, A. Kirchner, W. Williams, F. Heider, T. Leibl, and A. Hubert, *Geophys. J. Int.* **124**, 89 (1996).
- <sup>7</sup>Y. L. Hou, J. F. Yu, and S. Gao, *J. Mater. Chem.* **13**, 1983 (2003).
- <sup>8</sup>T. Hyeon, S. S. Lee, J. Park, Y. Chung, and H. Bin Na, *J. Am. Chem. Soc.* **123**, 12798 (2001).
- <sup>9</sup>S. H. Sun and H. Zeng, *J. Am. Chem. Soc.* **124**, 8204 (2002).
- <sup>10</sup>X. G. Peng, L. Manna, W. D. Yang, J. Wickham, E. Scher, A. Kadavanich, and A. P. Alivisatos, *Nature (London)* **404**, 59 (2000).
- <sup>11</sup>X. G. Peng, J. Wickham, and A. P. Alivisatos, *J. Am. Chem. Soc.* **120**, 5343 (1998).
- <sup>12</sup>F. Huang, H. Z. Zhang, and J. F. Banfield, *J. Phys. Chem. B* **107**, 10470 (2003).
- <sup>13</sup>F. Huang, H. Z. Zhang, and J. F. Banfield, *Nano Lett.* **3**, 373 (2003).
- <sup>14</sup>K. Lu, *Mater. Sci. Eng., R.* **16**, 161 (1996).
- <sup>15</sup>K. L. Thomas-Keprta *et al.*, *Geochim. Cosmochim. Acta* **64**, 4049 (2000).
- <sup>16</sup>C. B. Murray, S. H. Sun, W. Gaschler, H. Doyle, T. A. Betley, and C. R. Kagan, *IBM J. Res. Dev.* **45**, 47 (2001).
- <sup>17</sup>E. V. Shevchenko, D. V. Talapin, H. Schnablegger, A. Kornowski, O. Festin, P. Svedlindh, M. Haase, and H. Weller, *J. Am. Chem. Soc.* **125**, 9090 (2003).

- <sup>18</sup>E. Johansson and L. Nyborg, *Surf. Interface Anal.* **35**, 375 (2003).
- <sup>19</sup>E. Johansson and L. Nyborg, *Surf. Interface Anal.* **30**, 333 (2000).
- <sup>20</sup>B. Devouard, M. Posfai, X. Hua, D. A. Bazylinski, R. B. Frankel, and P. R. Buseck, *Am. Mineral.* **83**, 1387 (1998).
- <sup>21</sup>C. Tojo, M. C. Blanco, and M. A. Lopez-Quintela, *Langmuir* **13**, 4527 (1997).
- <sup>22</sup>C. Tojo, M. C. Blanco, and M. A. Lopez-Quintela, *Langmuir* **14**, 6835 (1998).
- <sup>23</sup>T. Sugimoto, *Adv. Colloid Interface Sci.* **28**, 65 (1987).
- <sup>24</sup>G. F. Goya, T. S. Berquo, F. C. Fonseca, and M. P. Morales, *J. Appl. Phys.* **94**, 3520 (2003).